NAIC-ID(RS)T-0128-96

NATIONAL AIR INTELLIGENCE CENTER

SELECTED ARTICLES

Approved for public release: distribution unlimited

DISCLAIMER NOTICE

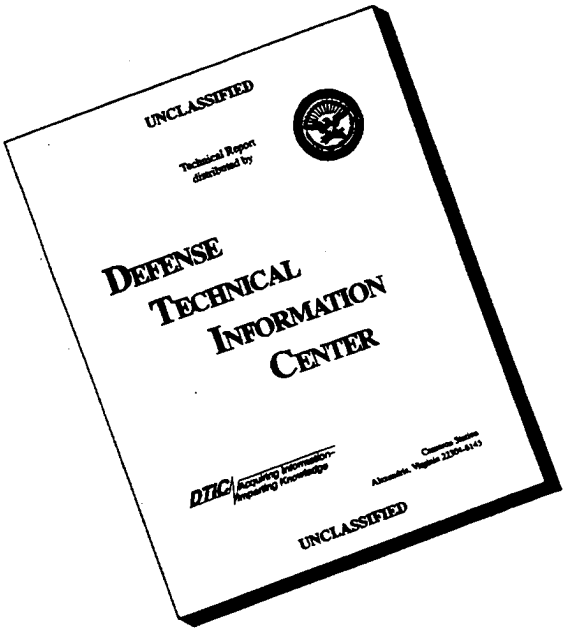

THIS DOCUMENT IS BEST QUALITY AVAILABLE. THE COPY FURNISHED TO DTIC CONTAINED A SIGNIFICANT NUMBER OF PAGES WHICH DO NOT REPRODUCE LEGIBLY.

HUMAN TRANSLATION

NAIC-ID(RS)T-0128-96 3 June 1996

MICROFICHE NR:

SELECTED ARTICLES

English pages: 40

Source: Qiangjiguang Yu Lizishu (High Power Laser and Particle Beams), Vol. 7, Nr. 4, November 1995; pp. 510-520; 543-548; 592-596.

Country of origin: China
Translated by: SCITRAN
F33657-84-D-0165
Requester: NAIC/TATD/Bruce Armstrong
Approved for public release: distribution unlimited.

TABLE OF CONTENTS

GRAPHICS DISCLAIMER

All figures, graphics, tables, equations, etc. merged into this translation were extracted from the best quality copy available.

CALIBRATION OF THE OPTICAL QUALITY OF A LARGE TELESCOPE SYSTEM

Wu Yi,Wang Yingjian,Wu Xubin

ABSTRACT Use is made of optical correlation functions associated with atmospheric trubulence to precisely determine turbulence optical correlation times. In conjunction with this--within these time periods--after atmospheric turbulence effects are corrected through imagery system optical transfer functions, large telescope (500mm aperture, 500m focal length) system optical quality is calibrated.

KEY WORDS Correlation function Turbulence Large telescope

0 INTRODUCTION

In experimental research during actual atmospheric laser transmission or imaging of celestial bodies through the atmosphere, it is often necessary for relatively large aperture and long focal length telescopes to be transmission or reception systems. The purposes are: 1) to increase beam transmission efficiency in order to reduce beam transmission diffraction angles; 2) to increase spacial resolutions associated with imaging systems. However, not only atmospheric turbulence effects will restrict their realization. Optical qualities of telescopes themselves are also an influencing factor. The reason is that it is very difficult for large telescope systems to reach ideal levels--that is, diffraction limitation systems. As a result, during the carrying out of experimental research using actual trubulent atmosphere as a transmission medium, there is a need to carry out calibrations on telescope system optical qualities. Normally, ideal system diffraction limitation multiples are used as characteristic. However, speaking in regard to large telescope systems--in particular, long focal length systems--it is very difficult, within the limited space of the laboratory, to carry out optical quality calibrations. There is a need to carry out this work in the actual atmosphere. Using the real atmosphere as background--when carrying out calibration of large system optical qualities--it is then necessary to experience influences associated with turbulence effects. As a result, there is a need to carry out corrections with regard to turbulence effects. Actual atmospheric turbulence often shows itself as a nonsteady random process. However, with respect to descriptions associated with turbulence effect optical parameters, their source is then steady random processes [1,2]. This article makes use of correlation functions associated with finite sequence random sampling in regard to turbulence effect optical parameters. First of all, precise determinations are made of correlation times associated with atmospheric turbulence. After that, within turbulence correlation time periods, long exposure statistics [1,2] are made with respect to atmospheric turbulence optical transfer functions ■OTF■. Finally, calibrations are achieved of large telescope system diffraction limitation multiples after turbulence effect corrections. The actual research object in this article is a 500mm aperture variable focal length Cassegrain telescope system developed by the Chinese Academy of Sciences Chengdu Photoelectric Institute.

1 EXPERIMENTAL PRINCIPLES

Fig.1 is a telescope system calibration experiment light path. The telescope has focus adjusted to 500m. CCD is used in recording light source imagery point spread functions and beam arrival angles calculated under the influence of turbulence effects. /511

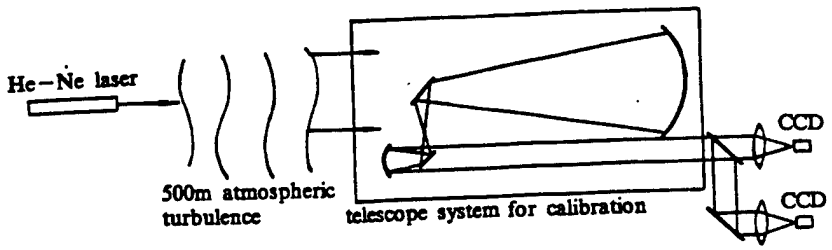

Fig.1 Experiment Optics

1.1 Telescope Diffraction Limitation Multiples

Taking telescopes and atmospheric turbulence together as an integrated imaging system forming images with regard to laser light sources at places 500 meters distant (approximating a point light source), light striation point spread functions on CCD image surfaces at this time are:

$$PSF = PSF_{Tur} * PSF_{Tel} \tag{1}$$

In this, PSFTur is the atmospheric turbulence point spread function.
PSFTel is the telescope system point spread function. * stands for scroll product. The modulation transfer function is the Fourier transform mode [3] associated with point spread functions, that is

$$MTF = |OTF| = F(PSF) \tag{2}$$

F( ) stands for Fourier transform. Therefore

$$MTF_{Tel} = \frac{MTF}{MTF_{Tur}} \tag{3}$$

MTF is obtained by the Fourier transform of imagery surface point spread functions. During long exposure statistics by turbulence optical statistics theory, MTFTur is then [2]

$$MTF_{Tur} = \exp[-3.44(\frac{D}{r_0})^{5/3}u^{5/3}] \tag{4}$$

In this, D is telescope diameter, ro is atmospheric turbulence

coherence length. u=fkλ/D is normalized spacial frequency. f is focal length. k is spacial frequency. λ=0.6328μm. Ideal telescope imaging system modulation transfer functions are [2]

$$\mathrm{MTF}_{T_0}=\frac{2}{\pi}\left(\cos^{-1}u-u\sqrt{1-u^2}\right) \tag{5}$$

The cut off spacial frequency is kc(u=1)=D/(fλ). Resolving power is

$$R_0=4\left(\frac{D}{\lambda}\right)^2\int_0^1 u\left(\cos^{-1}u-u\sqrt{1-u^2}\right)du \tag{6}$$

Actual telescope system spacial resolution is [2]

$$R=2\pi\left(\frac{D}{\lambda}\right)^2\int_0^1 u\mathrm{MTF}_{\mathrm{Tel}}(u)du \tag{7}$$

Therefore, telescope system diffractive limitation multiples can be precisely determined from the equation below

$$B=\left(\frac{R_0}{R}\right)^{1/2}=\left\{\frac{2\int_0^1 u\left(\cos^{-1}u-u\sqrt{1-u^2}\right)du}{\pi\int_0^1 u\mathrm{MTF}_{\mathrm{Tel}}(u)du}\right\}^{1/2} \tag{8}$$

1.2 Precise Determination of Atmospheric Turbulence Correlation Time Periods /512

We know that theoretical descriptions with regard to atmospheric turbulence optical parameters are based on steady random processes [1]. Due to the fact that actual atmospheric turbulence is often a nonsteady random process, it is necessary, as a result, to carry out statistical descriptions with respect to atmospheric turbulence optical parameters under a presupposition finite steady random processes. It is generally believed that this operation should be carried out within turbulence effect correlation time periods. Fluctuations in beam arrival angles and their correlation functions have the relationship below [1]

$$\int_{-\infty}^{\infty}B(\tau)e^{-i\omega\tau}d\tau=\left|\int_{-\infty}^{\infty}f_\alpha(t)e^{-i\omega t}dt\right|^{1/2} \tag{9}$$

In this, B(τ) is the turbulence optical correlation function. fα(t) is a time function associated with oscillations in beam arrival angles. The equation above clearly shows that power

spectra associated with oscillations in arrival angles are equal to Fourier transforms of correlation functions. This article makes use of sampling sequences associated with light striations on CCD image surfaces. Calculations are made of beam arrival angle time period sequences, and, in conjunction with that, discrete Fourier transforms are carried out on them. After that, use is made of discrete forms of equations above to carry out Fourier inverse transforms, obtaining the atmospheric turbulence optical correlation function $B(\tau)$. It is generally believed that, when $B(\tau)$ drops down to be zero, the corresponding time τo it the turbulence correlation time.

2 EXPERIMENTAL PARAMETERS AND RESULTS

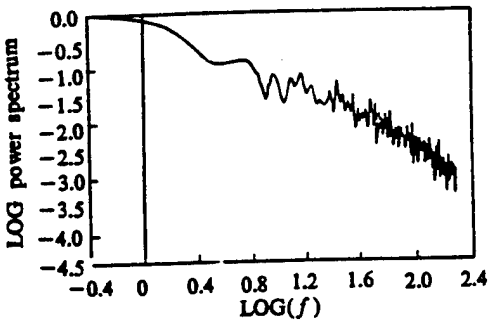

Fig.2(a) Power spectrum of arrival-angles

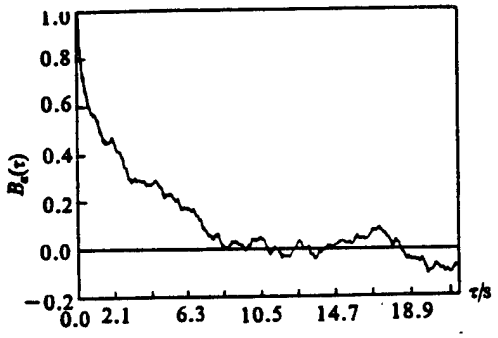

Fig.2(b) Correlation function from power spectrum of arrival-angles

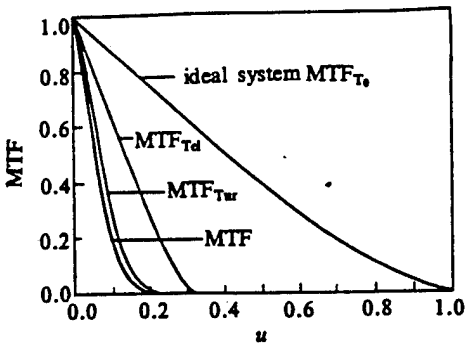

Fig.3 MTFs with normalized spatial frequence

In accordance with Fig.1, a 1mm He-Ne small aperture laser is shot out through 500m of turbulent atmosphere and received at telescopes. Through lenses, light striations form imagery on CCD image surfaces. At this time, due to the fact that light source small aperture dimensions are already smaller than 500mm aperture ideal systems associated with limit resolution scales at 500m distances, it is, therefore, possible to approximate their being point light sources. Optical striation point spread functions associated with CCD image surfaces are desribed by equation (1). Lens focal length is 450mm. During experiments, at the same time, option is made for the use of two CCD units to record optical striation imagery. The sampling frequency is 380Hz. Continuous recording of 8192 frames is used in obtaining arrival angle oscillation power spectra and atmospheric turbulence optical correlation functions. Due to the fact that the sampling frequency is fast, it is possible--after going through high speed Fourier transforms of 8192 discrete data--to obtain arrival angle oscillations power spectra associated with frequencies that are 0.045-190Hz. At the same time, from variances associated with arrival angle oscillations, it is possible to obtain turbulence lateral coherence length [3,4]

$$r_0 = 0.545 D^{-1/5} \lambda^{6/5} \langle f_\alpha^2 \rangle^{-3/5} \qquad (10)$$

$f\alpha$ is arrival angle. Experimental value associated with ro is 90mm. Fig. 2(a) is power spectra associated with arrival angle oscillations. Fig. 2(b) is atmospheric turbulence normalized correlation functions solved for from discrete forms associated with equation (9) on the basis of Fig. 2(a) data. From the Fig.'s in question, it is possible to see that--at 11 seconds--correlation function curves show the appearance of negative values (not due to measurement fluctuations)--that is, negative correlation. Therefore, turbulence correlation time is selected as 11 seconds. The sampling frame frequency associated with the second CCD unit is

10Hz. However, the image element resolution is higher than the former. It is used in obtaining imagery system modulation transfer functions MTF. From a summation of 110 frames of optical striation imagery within 11 seconds, average FFT obtain long exposure MTF. From equation (4), calculations are done of atmospheric turbulence modulation transfer functions MTFTur in long exposure situations. Fig.3 gives curves associated with long exposure MTF and long exposure MTFTur. Finally, from equation (3), solutions are made for
telescope system MTFTel--after long exposure average turbulence effect corrections--as shown in Fig.3. From equation (8), the telescope system diffraction limitation multiple B=3.087 is obtained.

3 CONCLUSIONS

In cases where corrections of the influences of atmospheric trubulence effects are considered, making use of square root reciprocal relationships associated with resolution specific values between optical imagery system spacial resolution and ideal system spacial resolution to precisely determine large telescope system diffraction limitation multiples is one effective means. In one area, it assists in our understanding optical qualities of actual telescope systems in order to quantify performance indices associated with sending systems as supplied by laser atmospheric transmission tests. In another area, the difficulties associated with carrying out indoor calibration of large telescope systems were resolved, and, in conjunction with that, methods were supplied to eliminate atmospheric turbulence effects.

REFERENCES

1 S.潘契夫. 谈镐生译. 随机函数与湍流, 北京: 科学出版社, 1976

2 Goodman J W. Statistical Optics. Wiley—Interscience Publication, 1985

3 Tyson R K. Principles of Adaptive Optics. Academic Press, 1991

4 Fried D L. Optical Resolution Through Randomly Inhomogeneous Medium for Very Long and Very Short Exposure. *JOSA*, 1966, **56**:1372~1379

MEASUREMENT OF WATER VAPOR CONTENT IN SINGLET OXYGEN GENERATOR BY SPECTROMETRIC METHODS

ABSTRACT Water vapor content is one of the important performance parameters associated with chemical singlet oxygen generators (SOG). Because it not only has a quenching effect on $O_2(1\Delta)$ but also has a severe quenching effect with regard to I* in oxygen iodine chemical laser (COIL) optical cavities, as a result, the measurement and control of water vapor content at SOG exit locations has important significance. The experiments in question opt for the use of optical spectrum strength comparison methods to measure water vapor content amounts in SOG. Making use of two dimensional scanning and accumulating functions of OMA-3, it is possible to carry out simultaneous scanning and accumulation with respect to optical spectra at different measurement points. Thus, it is possible to carry out water vapor amount determinations with regard to a number of individual SOG measurement points at the same time. Test measurement precisions can reach ±10%.

KEY WORDS Water vapor Singlet oxygen generator Spectrometric method

Cui Tieji Zhang Yunlu Min Xiangde Sang Fengting Sun Yizhu

Chen Wenwu Pang Jingke Jin Yuqi Yang Bailing

0 INTRODUCTION

The overall level associated with oxygen iodine lasers (COIL)[1] shows up primarily in performance levels associated with singlet oxygen generators (SOG) and media energy sources of the systems in question, adopted efficiencies associated with laser cavity structure with regard to laser media energies, and I2 generator performance. As far as O2(1Δ) concentrations produced in chemical SOG, which COIL's opt for the use of, are concerned, water vapor and residual oxygen content are primary indices measuring SOG performance. This article will make additional discussions with respect to water vapor amount measurement methods.

Although there are a relatively large number of methods to measure water vapor content, most of them are comparatively difficult. Primarily, they include absorption spectrometric methods--for example, spectrophotometric methods [3], and diode laser spectrometer methods [4]. The former makes use of 20m long absorption pools with wave lengths of 5900nm and time period response differences. Moreover, the instrumentation equiment associated with the latter is very expensive. However, its test measurement precisions are relatively high, and it is capable of acting as contrast standard. There is also one type that is a hygroscopic solid hygrometer method [5]. It requires that poisonous gases cannot be contained in gas flows. As a result, it is very difficult to apply it to COIL in SOG. Comparatively speaking, the best method is to make use of comaparative /516 methodsassociated with spectral line strengths [4]. It is relativelysimple. Response is fast, and it is comparatively easy to make use of on site. This article opts for the use of optical multichannel analyzers OMA. They are capable of simultaneously measuring spectral line strengths.

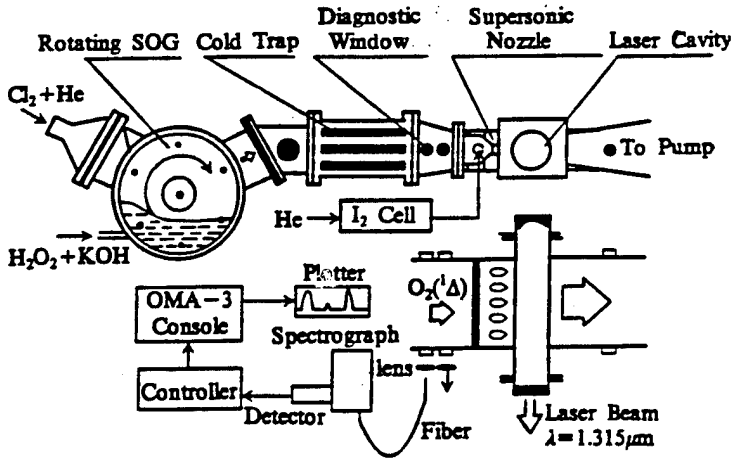

Fig.1 Schematic of cw supersonic COIL setup

These experiments opt for the use of experimental apparatus like that shown in Fig.1. In rotating SOG, first of all, premixed basic hydrogen peroxide BHP solution is added in. This can be prepared in accordance with fixed proportions from aqueous solutions of metallic hydroxides MOH such as Li, Na, K, and so on, and H2O2 (concentration generally is 35-90%). In this way--in BHP solutions---there necessarily exists quite an amount of liquid water. In conjunction with this, when Cl2 is added in, on BHP liquid film surfaces which are attached onto rotating disks and continually renewed, intense exothermic chemical reactions are generated, producing $O2(^1\Delta)$. At the same time, H2O is also produced

$$H_2O_2 + 2MOH + Cl_2 \rightarrow O_2(^1\Delta) + 2MCl + 2H_2O \qquad (1)$$

Large amounts of reaction heat will cause precooled BHP to violently rise in temperature, thereby producing a certain amount of H2O and H2O2 vapors as well as small liquid droplets and dilute gases flowing out together. Although, when droplets and water vapor go through SOG exit cold traps, the majority of them can be cooled out, from the time of their formation onward, however, there will then be certain gas phase and liquid phase quenching effects with regard to $O2(1\Delta)$ and so on.

In COIL activation media, water vapor is also very

harmful[2]. It is not only capable of making the speed of I2 molecule dissociation drop. It is also capable of making I* produce severe gas phase quenching. Going a step further, COIL performance is made to drop--even to the point of being unable to produce light. For this reason, it is necessary to strictly measure and control water vapor amounts in SOG.

1 MEASUREMENT PRINCIPLES AND EXPERIMENTS

In gas flows at SOG exits, concnetrations of O2(1 Δ) are capable of reaching 50-90%. In gas flows--at the same time--there also exist small amounts of H2O, H2O2, Cl2, O2(1Σ), as well as O2(3Σ), and other such gases. During the transmission process, they will give rise to the reactions set out below

$$O_2(^1\Delta)+O_2(^1\Delta)\rightarrow O_2(^1\Sigma)+O_2(^3\Sigma) \quad (2)$$

K1 = 2.0x10-17 cm3 / molecule • s, Reference [6].

$$O_2(^1\Delta)+O_2(^1\Delta)\rightarrow 2O_2(^3\Sigma)+h\nu\ ,\ 634\text{nm} \quad (3)$$

K2 = 4.4x10-23 cm3 / molecule • s, Reference [7].

$$O_2(^1\Sigma)+H_2O\rightarrow O_2(^1\Delta)+H_2O \quad (4)$$

/517

K3 = 5.5x10-12 cm3 / molecule v6,34 s, Reference [6].

$$O_2(^1\Sigma) \rightarrow O_2(^3\Sigma) + h\nu \ , \ 762\text{nm} \qquad (5)$$

A1 = 0.077s-1 , Reference [8].

Reaction (2) is a formula for the reaction producing O2(1Σ). The production rate is

$$v_1 = K_1[O_2(^1\Delta)]^2 \qquad (6)$$

Reaction (4) represents the quenching path associated with O2(1Σ) in SOG. In reality, there are such collision quenching companions as H2O, H2O2, Cl2, O2(3Σ), He, and so on. The ratios of their quenching speed constants [9] with respect to O2(1Σ) are 7x105:3x104:200:4:1. When temperatures are approximately 273K, due to the fact that H2O saturated steam pressure is 16 times H2O2, and speed constants are also close to ten fold, quenching effects associated with H2O2 are, therefore, capable of being left out of calculations. In analogous manners, as far as other quenching companions are concerned, it is possible to reach this conclusion. As a result, it is possible to recognize that, among SOG products, it is gaseous phase H2O that plays the decisive role in quenching with respect to O2(1Σ). Therefore, collision quenching speeds associated with O2(1Σ) can be written as

$$v_3 = K_3[O_2(^1\Sigma)][H_2O] \qquad (7)$$

Going a step further, it is possible to write out the dynamic equilibrium form associated with O2(1Σ)

$$d[O_2(^1\Sigma)]/dt = K_1[O_2(^1\Delta)]^2 - K_3[O_2(^1\Sigma)][H_2O] - A_1[O_2(^1\Sigma)] \qquad (8)$$

With regard to actual SOG systems, [H2O] is 1016 molecule/cm3 order of magnitude (1Torr, 273K). K3 = 5.5x10-12cm3/molecule • s and A1 = 0.077s-1 . One then has K3[H2O] >> A1 . Therefore, the final term in equation (8) is also capable of being ignored. When reaction systems reach equilibrium, then, d[O2(1Σ)]/dt=0. After rearrangement, one has

$$[H_2O] = K_1[O_2(^1\Delta)]^2/K_3[O_2(^1\Sigma)] \quad (9)$$

Luminescence strengths measured by OMA-3 probes for the two reactions (3) and (5) respectively are

$$I_{634} = \beta_{634} K_2[O_2(^1\Delta)]^2 \quad (10)$$

$$I_{762} = \beta_{762} A_1[O_2(^1\Sigma)] \quad (11)$$

β is the detection system spectral reception efficiency and sensitivity parameter. Use is required of standard light sources or other mthods for standardization. Taking (10) and (11) and substituting into (9), one has

$$[H_2O] = \{K_1/K_2\}\{A_1/K_3\}\{\beta_{762}/\beta_{634}\}\{I_{634}/I_{762}\} \quad (12)$$

Letting m={K1/K2}{A1/K3}{β762/β634}, then

$$[H_2O] = m\{I_{634}/I_{762}\} \quad (13)$$

m is overall system standardization constant. It is possible to obtain this from relatively precise standardized methods of doing test measurements on amounts of water vapor contained. Therefore, this method is simple and of practical use. However, its physical significance is not as clear as that of equation (12).

If use is made of (2), (4), and (5), as well as the reaction O2(1Δ) -> O2(3Σ) + hv (1270nm)--going through the same type of handling processes described above--it is also possible to obtain similar results to equation (12)

$$[H_2O] \propto (I_{1270})^2/I_{762} \quad (14)$$

In Fig.1, the mutual relationships between the measurement system in question and COIL are clearly shown. Optical radiation associated with reactions (3) and (5) collected from test measurement apertures is sent through optical fibers into spectral instruments associated with optical multichannel analyzer OMA-3 systems and shined onto narrow slits. In two dimensional probes OMA-3 is capable of carrying out simultaneous scanning and accumulation with respect to two spectral lines, thereby improving overall measurement time response and signal to noise ratios. Due to limiations associated with OMA-3 probe spectrum response ranges, it is only possible to make use of equation (12) to measure water concentrations. Fig.2 is scanning spectra for different amounts of water content associated with certain instants when Cl2 is poured into SOG. Using the

integration surface area ratio S634/S762 for wave lengths associated with the two spectral lines 634nm and 762nm to act as optical strenth ratio in equation (12), equation (13) then becomes

$$[H_2O] = mS_{634}/S_{762} \qquad (15)$$

/518

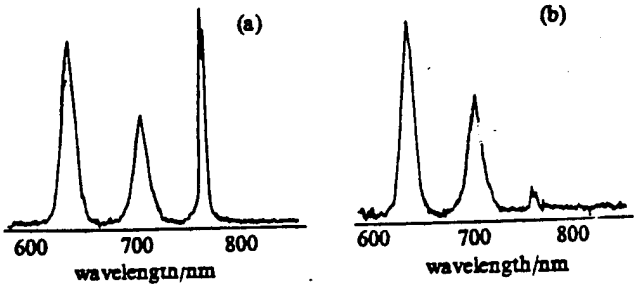

(a)Lower water content (b)Higher water content

Fig.2 The spectrum under different water content

Under normal experimental conditions, O2(1Δ) concentration changes produced by SOG in periods before and after experiments are not large. The lower [H2O] is, the larger spectral line surface areas associated with 762nm are--as is shown in Fig.2(a). When [H2O] is very low, the leading role of H2O among collision quenching companions of O2(1Σ) is also gradually yielded up to other companions. That is nothing else than to say that it is only necessary that KM[M] << K3[H2O] , that is, when

$$[H_2O] \gg K_M[M]/K_3 \qquad (16)$$

and then--and only then--are the conditions discussed above for ignoring those quenching companions satisfied. For example, when in the 273K range, the saturation pressure of the second main quenching companion H2O2 is 0.3 Torr. Selecting appropriate quenching speed constants [9], from equation (16), it is possible to obtain water vapor partial pressures much greater than 0.015 Torr. If calculations are done in accordance with 10 fold, water partial pressures should be at least > 0.15 Torr. Only at this time are the results obtained by equation (12) comparatively precise.

If [H2O] gradually increases--as is shown in Fig.2(b)--then, 762nm spectral line areas are gradually smaller until they are submerged in the signal to noise ratio. At this time, measurement errors enlarge. When [H2O] increases to partial pressures exceeding 3-5 Torr, 762nm spectral lines will then be difficult to resolve. For this reason, it is possible to obtain suitable ranges for the test measurement methods in question

which should be in the interval where water partial pressures are 0.1-5 Torr.

2 RESULTS AND DISCUSSION

SOG developed in previous periods opted for the use of tube type dry ice cold traps. After adequate BHP solutions were added, it was possible to make 3-4 iterations of tests. Each iteration was 2-4 seconds. The iterval between iterations was around 1-10 minutes. Average water content results for three continuous iterations of tests were, respectively, 0.88, 1.05, and 1.30 Torr. Later, SOG structures were improved. Option was made for refrigerator-alcohol cold traps. In conjunction with this, working under certain types of operational methods, average water content amounts associated with three continuous iterations of tests were 0.36, 0.24, and 0.19 Torr. With liquid nitrogen (LN2) cold traps, option is made for certain methods of pouring LN2. Results were 0.35, 0.60, and 0.74 Torr. From among experimental results, it was discovered that LN2 cold traps have better cooling results than dry ice cold traps. Moreover, water content amounts associated with test measurements for LN2 and dry ice cold traps follow along with the number of experimental iterations and drop. This is because cold trap efficiencies are in the process of falling. With refrigerator-alcohol cold traps, water content amounts follow along with the number of test iterations and go down. This is because cold trap efficiencies are in the process of going up. It was also discovered that there is an intimate relationship between such things as water content amounts associated with the latter periods of the same experimental iteration , average water content amounts and SOG structures, flow amounts and operating conditions, etc.

The test measurement methods in question make use of optical fibers, taking optical radiation associated with measured points and--using the same type of conditions--introducing OMA-3 probes. To this end, measurement instruments can be quite far away from COIL equipment measurement points. Because of OMA-3, it is possible to carry out simultaneous scanning, accumulation, and sampling of different spectra at the same location, thereby avoiding using two sensors and errors which are brought in when two light paths are measured. On the basis of OMA-3 two dimensional scanning functions, it is possible to take optical radiation associated with the same location (for example, in front of and behind cold traps or other important locations to study), and, using optical fiber, introduce OMA-3 probes at /519 different sites at the same time. Scanning and accumulation is done with regard to optical radiation signals associated with different sites (time intervals are capable of reaching a few tens of milliseconds). Thus, it is possible to measure water vapor amounts contained at various measurement points at the same time. Going a step further, one obtains, for instance, such results as cold trap efficiencies and so on, supplying data for evaluations with regard to SOG performance as well as COIL

levels.

From the principles of test measurement methods, it is possible to know that spectrometric methods are not able to measure water in condensed states which is capable of existing in SOG.

Acknowledgements: Participating in this experimental research, there were also such comrades as Shen Huihua, Li Mingsheng, Wang Dongmei, Liao Weiguang, Cong Jiagang, and so on. For this, we express our thanks.

REFERENCES

1 桑凤亭等. 强激光与粒子束, 1993, 5(3):389

2 Zagidullin M V *et al. Sov J Quantum Electron*, 1987, 17(3):320

3 Bonnet J *et al. Appl Phys Lett*, 1984, 45(10):1009

4 Barnault B *et al.* Eighth International Symposium on Gas Flow and Chemical Lasers, SPIE, 1990, 1397:231

5 Georges E *et al.* ONERA, BP72, 92322 Chatillon Cedex, France, 1994, Private communication

6 Heidner R F Ⅲ *et al. J Phys Chem*, 1983, 87(13):2348

7 Fisk G A *et al. J Chem Phys*, 1983, 77(10):4965

8 Heidner R F Ⅲ *et al. J Chem Phys*, 1981, 74(10):5618

9 王乃彦主编. 新兴的强激光, 北京: 原子能出版社, 1992, 183

EFFECT OF ATMOSPHERIC TURBULENCE ON PRECISION OF LASER TRACKING SYSTEM

Fan Chengyu Song Zhengfang

ABSTRACT This article discusses the influences of atmospheric turbulence on laser tracking system angular precision. Use is made of phase screen methods to calculate errors given rise to by atmospheric turbulence with regard to laser tracking systems. Calculations clearly show that, under normal conditions, tracking errors given rise to by atmospheric turbulence are capable of reaching several tens of microradians.

KEY WORDS Intensity fluctuation Phase fluctuation Tracking error

0 INTRODUCTION

In photoelectric systems where there is a need to precisely determine such things as target position, long range laser collimation associated with angular coordinates [1], as well as tracking systems, and so on, use is normally made of laser tracking detection systems. In References [3] and [4], the tracking errors have already been discussed in detail. However, only tracking errors given rise to by dark electric current, electronic circuit, thermal noise, and phase fluctuations were principally involved. It was believed that the influences given rise to by intensity fluctuations created by atmospheric turbulence were certainly not large. However, during actual applications, it was discovered that the influences of intensity fluctuations were very severe. In particuler, in situations associated with low angle of elevation real time tracking, tracking systems would often miss targets. Investigating the causes carefully, they are possibly due to the fact that, when solving for angular target miss amounts, the intensity distributions associated with optical faculae themselves are assumed to be uniform or presenting a Gaussian distribution. In the four quadrants, differences in light intensities are only due to distribution shares, that is, angular positions, being different. However, in reality--besides giving rise to phase fluctuations--atmospheric turbulence will also create light intensities making random distributions. This article will comprehensively consider the influences of phase fluctuations and light intensity fluctuations with regard to laser tracking system angular measurement precisions when beams are transmited through trubulent atmosphere. Initial results clearly show that the influences of turbulent atmosphere with respect to tracking errors will be larger than noise associated with detectors themselves. In particular, the influences of optical intensity fluctuations are larger. Under normal circumstances, tracking errors are capable of reaching several tens of microradians.

1 DETECTION PRINCIPLES

Option is made for the use of four quadrant photoelectric diode laser tracking principles as shown in Fig.1. Assuming that Gaussian beams are transmited through atmospheric turbulence to photoelectric detection devices as shown in Fig.1, if the coordinate origin point is selected at the center of incident light faculae, incident optical intensity distributions are

I(x,y). Then, the outputed electric current on each detector is [3]

$$i_k = \frac{\eta q}{h\nu} \iint_{A_k} I(x, y)\,dxdy \qquad (k = 1, 2, 3, 4) \tag{1}$$

/544

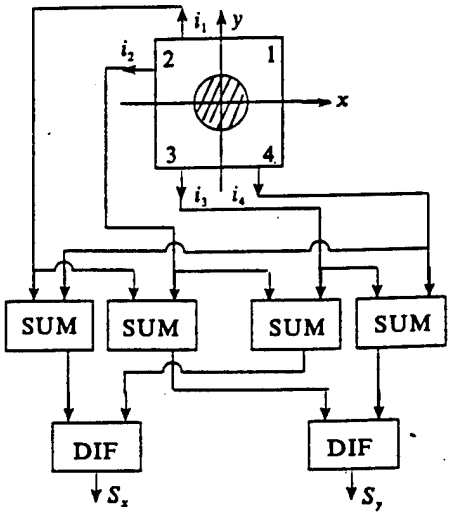

Fig.1 Quadrant detector system

Here,v is incident light frequency. η is quantum yield. h isPlanck's constant. q is electron charge. Ak is the faculae areaon the kth detector. In this way, the transmission signal in thex direction is

$$S_x = i_1 + i_4 - i_2 - i_3 \qquad (2)$$

The transmission signal in the y direction is

$$S_y = i_1 + i_2 - i_3 - i_4 \qquad (3)$$

Angular target miss amounts are

$$\theta_x = K \frac{S_x}{S} \qquad (4)$$

$$\theta_y = K \frac{S_y}{S} \qquad (5)$$

Here, S=i1 + i2 + i3 + i4. K is a proportionality constant. It is obtained through zero noise signal situations and represents tracking system angular sensitivities.

Besides this, angular target miss amounts can also be represented as

$$\sqrt{2}\theta = \sqrt{2}K \frac{1}{S/N} \tag{6}$$

$\sqrt{2}$ stands for angular target miss amounts that are equal in x and y directions. S/N stands for signal to noise ratio. This clearly shows that it is possible to reduce tracking error through increasing tracking system signal to noise ratios. However, with regard to the influences of atmospheric turbulence, raising signal to noise ratios is to no avail.

2 ATMOSPHERIC TURBULENCE NOISE FORMS

We now consider the noise produced by turbulence when lasers are propogated in the atmosphere. In reality, atmospheric turbulence most certainly is not uniform. It includes a good number of types of nonuniform lens media [5]. The indices of refraction are random variables associated with time. Fluctuations in indices of refraction cause light waves to produce amplitude and phase fluctuations during their propogation. Under certain conditions, these fluctuations are enough to cause relatively large tracking errors.

Assume the angular error created by atmospheric turbulence is θt and that angular errors led to by phase fluctuations and light intensity fluctuations are, respectively, θs and θI. These two partial errors can be taken to be statistically independent. As a result, we have

$$\theta_t = (\theta_s^2 + \theta_I^2)^{1/2} \tag{7}$$

Below, the two types of errors are discussed respectively:

(1) Phase Fluctuation Due to phase fluctuations at reception apertures, beams will produce expansion and vibration.

This vibration and reception aperture focal length then determine instantaneous beam arrival angle variances [6]

$$\langle \alpha^2 \rangle = \frac{D_s(\rho)}{k^2 \rho^2} \tag{8}$$

Here, k=2π/λ. λ is wave length. ρ is reception aperture diameter. Ds(ρ) is phase structure function. Option is made for the use of Von Karman turbulence spectra. With regard to spherical waves, it is possible to represent them as

$$D_s(\rho) = 1.091\, C_n^2 k^2 L_T \rho^{5/3} [1 - 0.8048 (\frac{\rho}{L_0})^{1/3} + 0.136 (\frac{\rho}{L_0})^2] \tag{9}$$

In this way, arrival angle variances can be written as

$$\langle \alpha^2 \rangle = 1.048\, C_n^2 (\Delta A)^{-1/6} L_T [1 - 0.8048 (\frac{\rho}{{}_0L})^{1/3} + 0.136 (\frac{\rho}{{}_0L})^2] \tag{10}$$

/545

Here, C_n^2 is atmospheric turbulence structure constant. ΔA is reception aperture area. LT is target range. LO is turbulence outer scale. Establishment of the equations above assumes reception apertures larger than $\sqrt{\lambda L_T}$. Root mean square electrical currents on detectors are

$$i_c = \sqrt{4\langle \alpha^2 \rangle}\ \frac{i_1}{K} \tag{11}$$

Signal to noise ratios are:

$$\frac{S}{N} = \frac{2i_1}{i_c} \tag{12}$$

Therefore,

$$\sqrt{2}\theta_s = \sqrt{2\langle\alpha^2\rangle} = \{2.096 C_n^2 (\Delta A)^{-1/6} \; L_T[1 - 0.8048 \; (\frac{\rho}{L_0})^{1/3} + 0.136 \; (\frac{\rho}{L_0})^2]\}^{1/2} \tag{13}$$

(2) Light Intensity Fluctuations If we assume wave propogation in direction z, wave fields are written to be

$$\varphi = \psi \exp(-ikz) \tag{14}$$

Then, ψ can be represented by the use of parabolic form equation [7]

$$2ik\partial_z \psi + \Delta_\perp \psi + 2k^2 n_1 \psi = 0 \tag{15}$$

Here, n1 = n - <n> is index of refraction undulation. $\Delta_\perp = \partial_{xx} + \partial_{yy}$.

Taking extension media and dividing them up into a good number of thin layers with thickness δz, each thin layer can act as a random phase screen. Each screen only introduces an independent amount of phase change with regard to waves propogated in it, and amplitudes do not change. Amplitude changes depend on a good number of δz diffraction accumulations. As far as this time is concerned, phase correlation functions can be represented as

$$B_\theta(\rho_1, \rho_2) = k^2 \int\int_0^{\delta_z} \langle n_1(z, \rho_1) n_1(z', \rho_2) \rangle dz dz' = k^2 \delta_z A_n(\rho_1 - \rho_2) \tag{16}$$

Here ρ is the two dimensional position vector (x,y). An(ρ) is the correlation function associated with index of refraction fluctuations on plane x-y. It is also capable of using turbulent flow spectrum Φn(k) for representation as

$$A_n(\rho) = 2\pi k^2 \delta_z \iint \Phi_n(\vec{\kappa}, \kappa_z = 0) \exp(i\vec{\kappa} \cdot \vec{\rho}) d^2\vec{\kappa} \qquad (17)$$

As to processes associated with flow fields from one screen to another screen, it is possible to obtain them through solving equation (14). Assuming that n1 = 0, in the frequency spectrum realm, Ψ(z,k) is a two dimensional Fourier transform associated with ψ(x,y,z). In that case, equation (14)'s transformation is made into

$$\partial_z \Psi(z, \kappa) = -i \frac{\kappa^2}{2k} \Psi(z, \kappa) \qquad (18)$$

It has the solution

$$\Psi(z', \kappa) = \Psi(z, \kappa) \exp[-\frac{i\kappa^2 (z'-z)}{2k}], \qquad (19)$$

In this way, the process with regard to wave propogation through δz = z'-z in a random medium is

(a) $$\psi(z, \rho) = \psi(z-, \rho) \exp[-ik \int_0^{\delta_z} n_1(\rho, z'') dz''];$$

(b) discrete Fourier transform of ψ (z,ρ) to Ψ (z,k);

(c) $$\Psi(z'-, \kappa) = \Psi(z, \kappa) \exp[-\frac{i\kappa^2 (z'-z)}{2k}];$$

(d) inverse discrete Fourier transform of Ψ (z'-,k) to ψ (z'- ,ρ).

Here--as far as using (z'-,ρ) to represent wave field propogation to fields associated with point z in screens is concerned--this process is repeated with respect to all phase screens right up to wave fields arriving at observation planes. Finally, the squares are then selected--that is, representing light field distributions on detectors. Fig.2 and Fig.3 are then nothing else than optical intensity distribution graphs calculated out making use of phase screen methods. We only select data from middle sections. From the Fig.'s, it can be seen that they are remote Gaussian distributions. Making /546 use of this light intensity distribution, it is possible to calculate out θt . Again, making use of equation (7) or equation (13) to subtract the influences of phase fluctuations, that is, it is possible to calculate the influences of light intensity fluctuations on angular precisions.

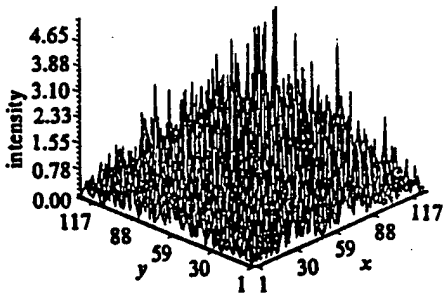

Fig.2 Intensity distribution

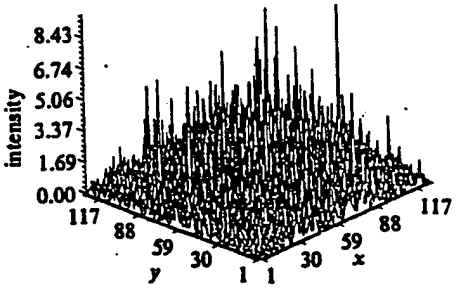

Fig.3 Intensity distribution

3 CALCULATION RESULTS AND CONCLUSIONS

We considered cases of horizontal laser propogation through the atmosphere. The transmiting laser wave length is 1.06μm. Divergence angles are 1.5mrad. Making use of Von Karman turbulence spectra, turbulence outside scales Lo are 2m. Inside scales are 0.01m. Reception apertures are 0.4m. As far as the influences of phase fluctuations on laser tracking systems are concerned, it is possible to make use of equation (12) to carry out calculations. As to the influences of intensity fluctuations, we assume that tracking systems have already been aligned on targets. Phase screen methods are used to calculate light intensity distributions on detectors. During calculations, we make use of 512x512 screens. Screen intervals are 100m. First of all, calculations are made of beam field distributions

through the first screen. On the basis of already known tracking distances, precise determinations are made for the number of screens through which light fields pass right up to obervation planes. Finally, calculations are made of light intensity distributions on observation planes. Giving consideration to limitations on reception apertures, we only select light field distribution data inside apertures. Making use of equations (4) and (5), calculations are done of the influences of atmospheric turbulence on laser tracking angular precisions. Here, the proportionality constant K = 1.473x10-4/f rad. Then, use is made of equation (7) to calculate out the influences of light intensity fluctuations. In calculations, first of all, it is assumed that transmission distances are fixed (distance is 5km). Turbulence intensities change. Calculation results are shown in Fig.4. After that, it is assumed that turbulent flow intensities are fixed. Transmission distances are varied. Results are seen in Fig.5. Table 1 sets out calculation results for θ_s and θ_i under these conditions. From Table 1, it is possible to know that tracking errors created by intensity fluctuations play the

Table 1 Tracking error induced by atmospheric turbulence

$C_n^2/m^{-2/3}$	1×10^{-15}		1×10^{-14}	
L_T/km	θ_s/μrad	θ_i/μrad	θ_s/μrad	θ_i/μrad
1	1.25	4.62	3.96	11.22
2	1.77	6.03	5.60	13.75
3	2.17	7.39	6.86	15.92
4	2.50	8.67	7.92	17.75
5	2.80	9.90	8.85	19.21
6	3.07	11.06	9.70	20.33
7	3.31	12.15	10.48	21.10
8	3.54	13.18	11.20	21.51
9	3.77	14.15	11.89	21.57
10	3.96	15.05	12.52	21.27

/547

dominant role. Tracking errors led to by phase fluctuations are--when turbulent flows are relatively weak--approximately one third of intensity fluctuations. Moreover, when turbulent flow strengths are medium, the difference between the two is somewhat reduced. The farther tracking distances are, the smaller the difference is. This phenomenon may possibly be created by saturation effects [6] associated with intensity fluctuations.

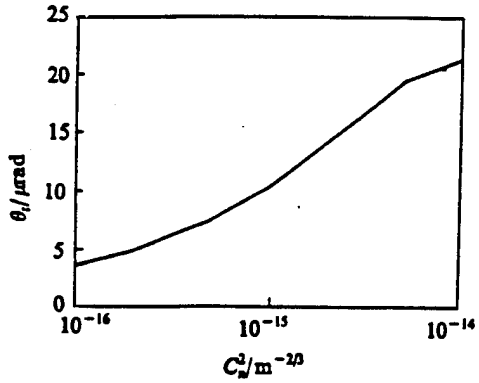

Fig.4 Tracking error vs turbulence

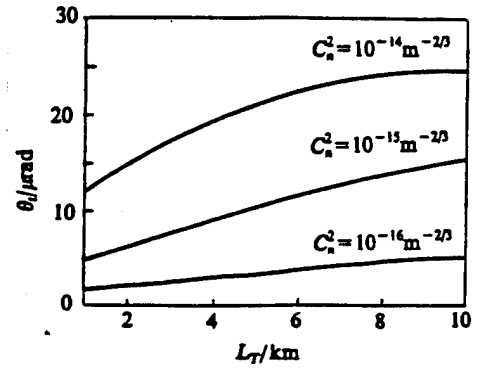

Fig.5 Tracking error vs range

On the basis of our observations, as far as turbulent flow strengths near the earth's surface are concerned, they are weak when under 10-16m-2/3. During normal clear weather, they are around 10-14m-2/3. When they are strong, they have the capability of reaching above 10-13m-2/3. From these Fig.'s, it is possible to see that--in cases where turbulent flows are weak--for distances inside 10km, tracking errors given rise to by atmospheric turbulence do not exceed 5μrad. In situations where turbulence is moderate, tracking errors reach 25μrad. If turbulence is even stronger, then, at close ranges, they are also

capable of exceeding 25μrad.

Speaking in terms of aerial target tracking, the higher altitudes are, the weaker turbulence is, and the smaller tracking errors are. However, the closer it is to the earth's surface, the stronger turbulence is. This is the case for no other reason than that--when angles of elevation are low--it is difficult to track. As to tracking errors which are created by turbulence in this case, we will discuss them again later.

Acknowledgements: Our thanks to Comrade Wang Yingjian for supplying laser atmospheric transmission numerical value simulation programs.

REFERENCES

1 Rands J F and Zankowsky D R. *Proc IEEE*, 1982, **70**: 635

2 Skolnik M I. Introduction to Radar Systems, New York: McGraw-Hill, 1980

3 Kazovsky L G. *Opt. Eng*, 1983, **22**: 339

4 Walter J E. Prospects for Precision Active Tracking Using a Quadrant Detector, AD-A022714, 1976

5 Strohbehn J W. Laser Beam Propagation in the Atmosphere. (Topics in applied physics; v. 25) New York, 1978

6 宋正方. 应用大气光学基础, 北京: 气象出版社, 1990

7 Martin J M and Flatte S M. *Appl. Opt*, 1988, **27**: 2111

EFFECTS OF COATING THICKNESS NON-UNIFORMITY ON FAR-FIELD PERFORMANCE OF BEAM INDICATOR

Xiong Shengming Zhang Yundong Wang Yongzhong

ABSTRACT Optical thin films in DF (deuterium fluoride) high power laser system beam directors are discussed. Use is made of polarization ray trace to analyze polarization state changes in main lasers and beacons at director pupils. Calculations are made of the influences of coating thickness nonuniformities on far field performance.

KEY WORDS High power laser Beam director Multilayer coastings Coating thickness nonuniformity Far field performance

0 INTRODUCTION

High power laser systems require that--in optical components--use be made of muliple layer optical coatings to make their high efficiency output laser energies. On optical surfaces which have curvatures, incident angles across optical apertures continuously change. In particular, within incident angle ranges associated with beam expander device reflector surfaces, reflectance changes (Rs and Rp) are not obvious. However, as far as across apertures on the same reflectors is concerned, incidence angles continuously change and optical coating reflectances as well as reflection phases change following along with wave length. On entire mirror surfaces, phase extensions Δ ($\phi s - \phi p$) change following along with incidence angles and wave lengths. Small coating thickness changes will still lead to obvious Δ changes [1,2].

In large aperture laser emission systems, as far as sensing devices which are sensitive to polarization are concerned--for example, interferometers, wavefront sensors, tracking devices, and so on--in measurements of such data with regard to wavefronts, it is necessary with respect to entire light path systems to complete polarizaton analyses of them from beginning to end. As far as light paths associated with multiple layer optical coating optical components and possessing coating thickness changes are concerned, coating thickness changes are capable of giving rise to wavefront changes associated with peak and valley differences which reach a wave length. If, in regard to wavefront detection, use is made of light wave and emitted laser light wave lengths which are not the same, as a result, wavefronts measured by wavefront sensor devices are not the same in wavefront errors [3] associated with emitted laser light undergoing the same light path. Detected wavefronts and emitted laser light wavefronts change following along with incidence angle and laser operating time developments.

This article discusses optical coatings used by DF high power laser systems. It uses polarized light ray trace analysis on pupil polarization changes and calculates the influences of coating thickness nonuniformities on far field performance.

1 REFLECTOR FILM SYSTEMS AND CHARACTERISITCS

Based on overall optical system requirements, we opt for the

use of metallic media strengthened film systems. The design of the entire film system is Sub/CrAg (PbF2/ZnSe)3/Air. In it,/593

Ag thickness is 100nm. PbF2 and ZnSe optical thicknesses are 1/4 of 3.8μm. Fig.1 gives visible and infrared theoretical spectrum curves associated with this type of coating system design. On the basis of currently available film plating equipment as well as film plating technology, in beam directors, Φ600 main reflector coating thickness change is 5%-6%. Secondary reflector film thickness change is adopted as 3%. Coating thickness distributions have their source in the calculations of Reference [2]. Fig.2 is beam director main reflector coating thickness distribution forms. In high power laser transmission systems, other optical component coat ng thickness distribution forms are analogous to this.

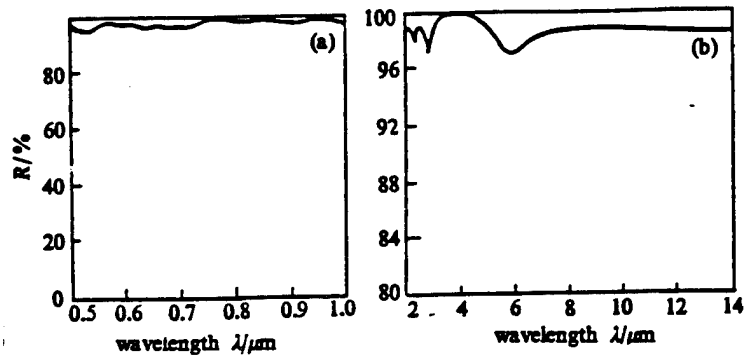

Fig.1 Theoretical reflectance spectral for coating Sub/CrAg (PbF2/ZnSe)3/Air

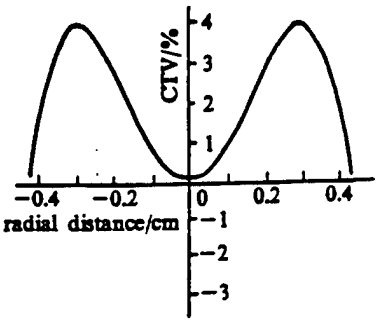

Fig.2 Coating thickness variation model of primary mirror of director

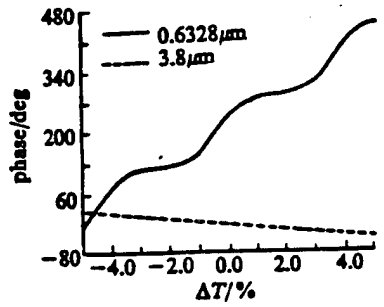

Fig.3 Phase variation due to nonuniformity for standard quarterwave design

In multiple layer coating systems, small coating thickness variations (CTV) will give rise to large equivalent surface form errors. Surface form errors which are given rise to by coating thickness variations are produced by reflected light phases because reflected light phases are functions of coating thickness. Fig.3 represents reflected light phase changes given rise to by coating thickness variations. In the Fig., angle of incidence is 15°. Reflectance of 3.8μm wave length laser light is 99.9%. Below, we will investigate the sensitivities of system properties to these changes.

In studies, it is assumed that coating thickness varies along with radial direction changes and rotations are symmetrical. Coating thickness variations are dependent on optical component size, the geometrical dimensions of coating plating machines, and other plating techniques. In situations where multiple high reflectance coatings have coating thickness variations, reflectance changes are very small. However, reflected light phases are capable of changing several hundred degrees.

2 POLARIZATION ANALYSIS

Before we do some work, there is still no polarization analysis software inside China which is capable of handling thin films that possess coating thickness variations associated with

symmetrical rotations. As far as our writing of polarized light ray trace computer software is concerned, use was made of analytical methods associated with Jones calculations [4] and Eugene Waluschk's discussions [5]. This software studies the taking of each polarized component (each component in a light path) and dividing it into a combination of parts that are polarization devices and delay devices. Polarization device light axses are parallel to the beam and the plane s of the optical surface affecting it. Delay device light axses are parallel to the plane p.

Reflector polarization device matrix primary transmission rates are Rs = r_s^2, and Rp = r_p^2 . Rs and Rp are, respectively, s- an: p- component reflectances. ϕs and ϕp are plated coating reflector s- and p- component reflection phases. Polarization device matrices are complex numbers. Generally, rpi

≠ rsi . Selecting the incident surface included angle /594 between reflectors to be θi, reflection matrices associated with various reflectors are

$$M = \begin{bmatrix} r_s e^{i\varphi_s} & 0 \\ 0 & r_p e^{i\varphi_p} \end{bmatrix}$$

Conversion matrices associated with light rays entering into reflector corrdinates are

$$R(\theta_i) = \begin{bmatrix} \cos\theta_i & \sin\theta_i \\ -\sin\theta_i & \cos\theta_i \end{bmatrix}$$

Reflector coordinate reconversion matrices are

$$R(-\theta_i) = \begin{bmatrix} \cos\theta_i & -\sin\theta_i \\ \sin\theta_i & \cos\theta_i \end{bmatrix}$$

Jones matrix calculations obtain an array of vectors. It is composed of two polarization states which are mutually perpendicular to each other with amplitude and phase being, respectively, Ax, 8,45
x, Ay, ϕy

$$J = \begin{bmatrix} A_x e^{i\varphi_x} \\ A_y e^{i\varphi_y} \end{bmatrix}$$

In order to precisely determine the influences of thin films on surfaces with curvatures as well as the influences of coating thickness variations on reflector accumulations, it is necessary to calculate Jones vectors associated with different aperture positions across laser systems. We are able to recognize that laser system pupils are two types of different apertures. One type is S polarized light apertures. The other type is P polarized apertures. Light wave polarization states inside the two apertures are mutually perpendicular. As far as carrying out calculations with regard to variations in amplitude and phase associated with the two apertures is concerned, two dimensional Fourier transforms are then carried out on each aperture's wave surface. Far field strength distributions are then obtained. The two polarization state far field strength distributions are then added together. Eliminating 2, overall strength distributions are then obtained. The ratios between far field

strength distribution center faculae intensities and ideal system central faculae intensities are Strehl ratios.

3 CALCULATION RESULTS

On reflectors, multiple layer optical coatings will give rise to reflected light phase delay variations, thereby leading to obvious polarization and wave front changes. For this reason, we calculated polarization state variations and far field strength distributions in pupils associated with different wave lengths of beam director light waves. In calculations, main reflector coating thickness variations are selected as 5%. Secondary mirror coating thickness variations are selected as 3%.

Coating systems are the same as strengthened metallic media reflection coatings. In calculations, consideration has not yet been given to chromatic dispersion with regard to different wave lengths and media coating layers. Fig.4 represents horizontal ray polarized incident 3.8μm wave length laser light in two cases of pupil polarization state changes--beam director reflectors with and without coating thickness variations. Fig.5 is pupil polarization state changes associated with 0.6328μm beacon light. Fig.6 and Fig.7 are, respectively, far field intensity distributions at beam directors associated with 3.8μm intensity light and 0.6328μm becon light. Table 1 summarizes

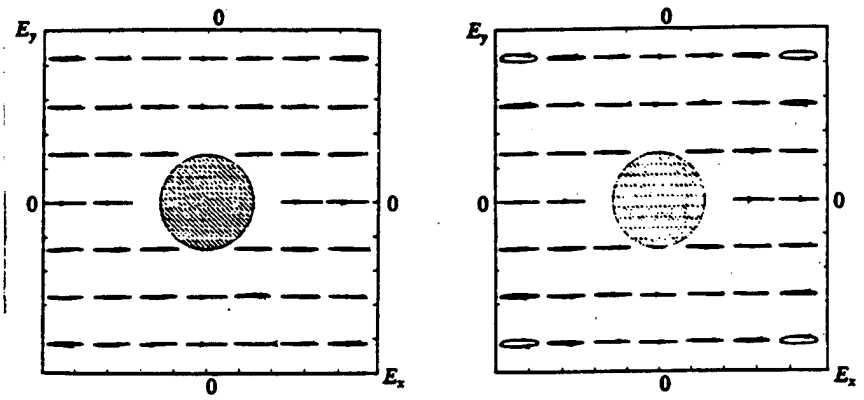

Fig.4 The polarization state of 3.8μm laser at the pupil of director (a) Without coating thickness variation (b) Coating thickness variation (main mirror 5%, secondary mirror 3%) /595

the influences of coating thickness variations on three main spectral lines associated with DF laser light transmission and

beacon wave length light wave far field Strehl ratios.

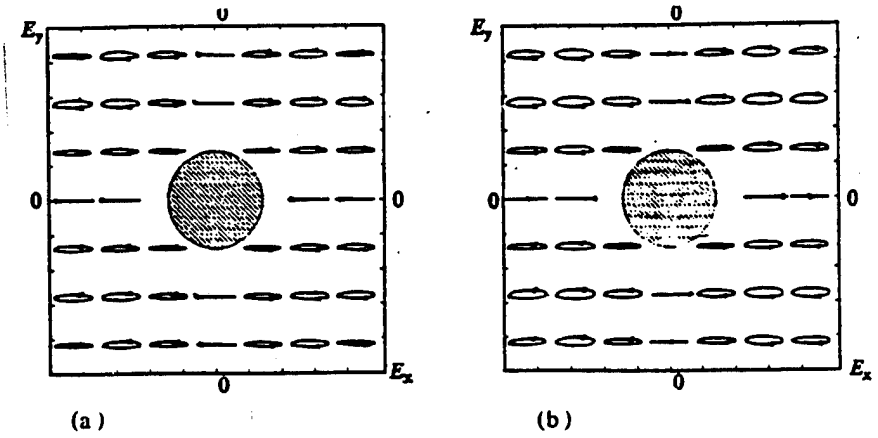

Fig5. The polarization state of 0.6328μm laser at the pupil of director (a) Without coating thickness variation (b) Coating thickness variation (main mirror 5%, secondary mirror 3%)

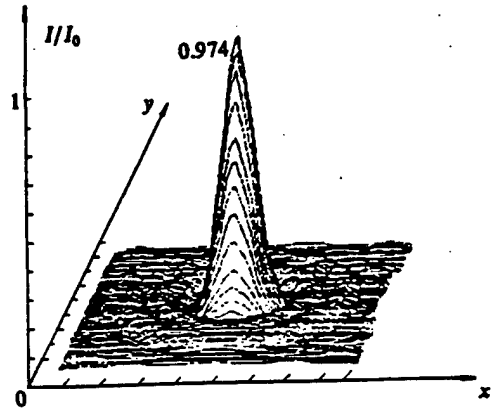

Fig.6 3.8μm laser far-field intensity distribution

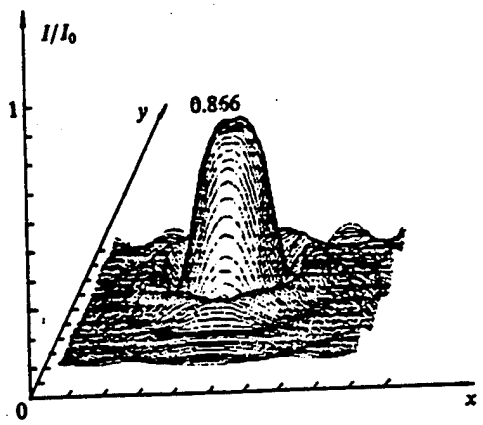

Fig.7 0.6328μm laser far-field intensity distribution

Table 1 Far field performance effects due to coating thickness variation (CTV)

wavelength / μm	0.6328	3.80	3.716	4.041
no CTV	0.9541	0.9941	0.9941	0.9941
5% CTV of primary mirror 3% CTV of secondary mirror	0.8504	0.9607	0.9498	0.9783

4 CONCLUSIONS

If laser systems do not carry out overall wavefront calibration, polarization effects given rise to by thin coatings will have obvious influences on wavefronts and far field performance. Due to multiple layer coating interference effects, wavefront errors undergone by main laser and beacon light are not the same. Looking at the calculation results above, influences of coating thickness variations on beacon light polarization and far field performance are much more severe than high power lasers. Using the calculations above, consideration was only made of two director reflectors. In the calculations above, option was made for the use of coating system polarizations that are relatively small. 0.6328μm wave length beacon light far field Strehl ratios then fall to 0.85. This already approaches the traditional Rayleigh criterion. In situations equivalent to 5% coating thickness variation, reflectors are not able to /596 exist to create errors.

If consideration is given to all reflectors associated with optical systems--in particular, those refraction transfer reflectors where coating thickness variations also exist--it will lead to severe polarization effects, producing image distortion and loss of focus [1]. Far field performance will drop a step further. As a result, there is a need to: (1) optimize coating system design, control phase delay across apertures, and reduce coating thickness variations, as well as the influences of incident angles on polarization and wavefronts; (2) optimize coating plating techniques, reducing coating thickness errors;

(3) go through entire system performance calculations to precisely determine coating thickness errors; (4) match up residual wavefront errors associated with high power lasers and beacon light.

REFERENCES

1 Dr Wasim Hasann and Dr Bruce A Tirri. *SPIE*, 1989, 1116

2 熊胜明、张云洞. 强激光与粒子束, 1992, 4 (1): 59 ~ 64

3 Guha J K, Paul W Scott and Southwel W H. *Applied Optics*, 1980, 19: 1320

4 Jones R C, A new calculus for the treatment of optical system, Reprinted in Swindell, Polarized Light, 1975

5 Eugene Waluschkc. *SPIE*, 1988, 891

6 Daniel J Reily, Russel A Chipman. *SPIE*, 1992, 1746